Granular Matter (2007) 9:295–307
DOI 10.1007/s10035-007-0047-1

Coexisting static and flowing regions in a centrifuging granular heap

T. Shinbrot · N.-H. Duong · M. Hettenbach · L. Kwan

Received: 24 July 2005 / Published online: 13 July 2007

Abstract We report an unexpectedly rich variety of new flow patterns on a granular heap that is centrifuged so as to simulate a reduction in gravity. These surface patterns exhibit coexisting static and flowing regions that depend strongly on centrifugal stress, but surprisingly not on mass flow rate. A discrete cellular automata model reproduces some of the patterning features and indicates that subsurface jamming may precipitate the formation of localized frozen patterns on the surface. This model provides insights into the mechanics of granular flows under controlled stress environment and jammed-to-flowing transitions in granular media.

Keywords Granular solidification · Granular fluidization · Cellular automata

1 Introduction

Granular responses to controlled stresses are not well understood. Over the years, attempts to address these responses under controlled laboratory conditions have been made in well-instrumented cells [1–7], chutes [8–14] and other systems [15–18]. Notwithstanding many important advances, understanding remains limited even in well characterized conditions, and is still more limited under uncommon conditions [19,20], for example in reduced gravity environments as will be encountered in future planetary explorations [7,21,22].

In previous work [21], we studied the effect of reducing the density of particles as a means of approximating the effect of reduced gravity on granular flows. In those experiments, we found evidence that the dimensionless ratio of particle settling speed to mean granular flow speed, R_{pt}, was a predictor of flow transitions. Prior researchers in Aeolian and fluvial flows have similarly concluded that the Rouse number (the ratio between terminal sedimentation velocity and fluid speed) governs transport and sedimentation. In our work, we found that when R_{pt} is large, particles settle rapidly and behave as we expect from observations of terrestrial granular flows. That is, grains fall rapidly and transition from one solid-like state to another, as does sand falling through an hourglass. On the other hand, when R_{pt} is small, grains remain fluidized for long periods, and granular flow more closely resembles fluid flow. Thus for small R_{pt}, grains form waves, slosh and reflect from boundaries, and leave behind fluvial-appearing sedimentary or erosional landforms. The picture that the character of granular flows may depend on simple dimensionless groups like R_{pt} is supported by reports that solid-like and fluid-like terrestrial particle-laden oceanic and volcanic flows are similarly correlated with the ratio between settling- and debris-flow speeds [23,24]. These combined results suggest that under reduced gravity—as is seen on Mars—grains may settle more slowly than on Earth, and consequently dry granular flows can produce surface features that, on Earth, would be interpreted as being caused by fluvial flows.

Reducing particle density as we have previously done is one way of reducing R_{pt}; on the other hand, arguably low density grains may be anomalously subject to complex air-particle interactions that may occur during settling [25,26]. Therefore in this paper, we explore a more controlled way of

T. Shinbrot (✉)
Department of Biomedical Engineering, Rutgers University,
599 Taylor Road, Piscataway, NJ 08854, USA
e-mail: shinbrot@soemail.rutgers.edu

N.-H. Duong · M. Hettenbach · L. Kwan
Department of Chemical and Biochemical Engineering,
Rutgers University, 98 Brett Road, Piscataway, NJ 08854, USA

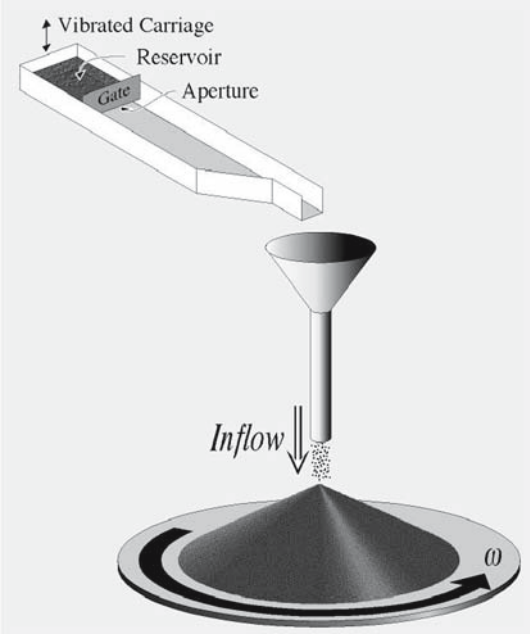

Fig. 1 Experimental arrangement for centrifuging granular heaps. Grains are uniformly metered from above at a prescribed mass flow rate, and the granular heap that forms can be centrifuged by adjusting the rotation speed, ω, of a supporting disk. Grains are uniformly metered through a ∼1 cm ID vertical tube as shown from a vibrated, slanted reservoir of grains with a gate valve of fixed aperture (Eriez Magnetics, Erie, PA). By altering the aperture or vibration amplitude, we can vary mass flow rates. Flow rates are steady to within about 10%, as measured by monitoring the mass of grains received in a container over a period of several minutes (the duration of a typical experimental trial). The grains used in the experiments that we describe here are solid glass spheres (Potter Industries, Valley Forge, PA) sieved between 45 and 90 μm in diameter; other experiments in which we have varied particle properties will be reported elsewhere

reducing R_{pt}, namely by centrifuging grains, thereby simultaneously decreasing the particle settling rate and increasing the mean flow rate. The arrangement that we use is depicted in Fig. 1, where we show a rotating granular heap on which a continuous inflow of grains is uniformly metered (see figure caption for description of metering apparatus).

Flow instabilities on spinning disks (e.g., in coating applications [27]) have previously been studied using both Newtonian and non-Newtonian fluids in centrifuging geometries [28,29]. These studies have revealed that fluid flows on spinning disks tend to generate uniform thickness films—exceptions include coiling of very viscous fluids [30], and evaporation-mediated fine striations that form at high speeds [31]. Centrifugation has also been reported in a limited number of granular experiments, e.g., to probe fracture of flat cakes of grains [32], to investigate the free surface of grains in a rotating bucket [33,33–35], and to explore spiral structures in settling grains in slurries [36–38].

In this paper our purpose is to use centrifugation to reduce the compressive loading of a heap produced by gravity, and thereby to improve the understanding of dynamical granular behaviors under reduced gravity conditions. In the sections following, we begin by deriving the stress at the surface of a granular heap on a spinning disk. We then describe patterns seen on the surface of grains on an experimental spinning disk. We next evaluate the dimensionless groups governing this problem, which we follow by constructing a cellular automata simulation of flow on the spinning disk. Finally, we prognosticate on possible avenues for future research in this system.

1.1 Stress analysis at surface of centrifuging heap

In Fig. 2a, we sketch the free body diagram for granular flow on a spinning disk. In that figure, we focus on a volume of material (upper left, inset) on a spinning surface inclined at an angle, ϑ, to the horizontal. As indicated in the inset, this volume feels a normal compressive acceleration of -g·cos(ϑ), balanced by a normal centrifugal acceleration of $+\omega^2 \mathrm{r} \cdot \sin(\vartheta)$, where ω is the angular rotation speed, g is the gravitational constant, and r is the radius from the center of the spinning disk. Consequently, at an inclined or heaped surface on a spinning disk, the compressive force per unit grain mass is summed to an effective value:

$$\mathrm{a_n} = \mathrm{g}\cos(\vartheta) - \omega^2 \mathrm{r}\sin(\vartheta), \tag{1}$$

and the tangential (downhill) force per unit mass is:

$$\mathrm{a_t} = \mathrm{g}\sin(\vartheta) + \omega^2 \mathrm{r} \cdot \cos(\vartheta) - \mu \mathrm{a_n}, \tag{2}$$

where μ is an effective friction coefficient of the grains. If the rotation speed is much larger than the radial flow speed, Coriolis effects can be neglected [39,40] and the compressive loading on grains can be inferred from the local radius and angle of the heap. Conversely, at steady state, if frictional losses are taken to exactly balance downstream acceleration, then (1) and (2) can be combined to give a relation between inclination angle, ϑ, and rotation rate, ω:

$$\vartheta = \tan^{-1}\left(\frac{\mu \mathrm{g} - \omega^2 \mathrm{r}}{\mathrm{g} + \mu\omega^2 \mathrm{r}}\right). \tag{3}$$

This is an elementary result from powder mechanics [41] with a straightforward embellishment to include centrifugal acceleration, and is plotted in Fig. 2b alongside experimental data. Experimental measurements of ϑ are evaluated by averaging the heap inclination angle obtained from digital photos taken from the side. To produce a theoretical comparison using Eq. (3), we use $\mu = 0.55$ and r = 5. The choice of μ is obtained by averaging experimental data at ω =0, and the choice of r is taken to minimize squared errors (and corresponds to about the middle of our experimental disk). For larger r, the theoretical curve is steeper, and for smaller r it is more shallow.

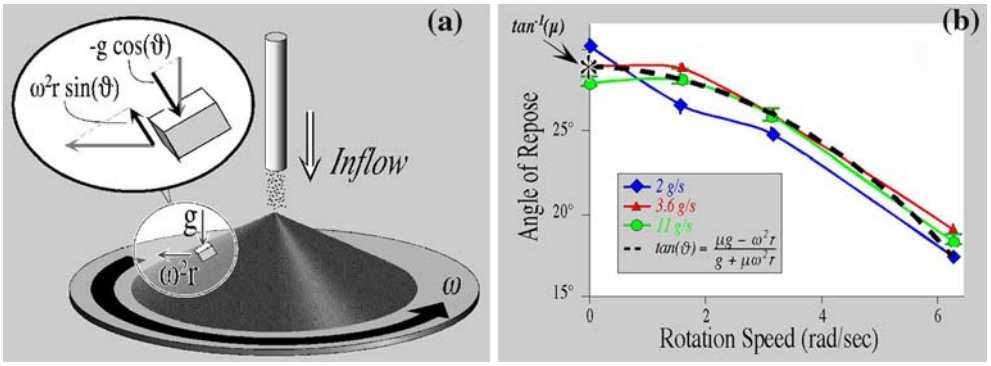

Fig. 2 **a** Schematic of a heap of grains on a spinning disk. Inset: component forces defined in Eq. (1) and (2) on a unit volume at the surface of the heap. Note that the normal component of the centrifugal acceleration acts to *oppose* the normal component at the heap surface due to gravity. **b** Resulting inclination angle of the free surface as a function of rotation speed measured for a few mass inflow rates, and for the best fit from Eq. (3). The fit is consistent with Eqs. (1)–(3), confirming the elementary derivation that centrifugation opposes gravitational compressive stress on the heap

Evidently, Eq. (3) reasonably approximates the slopes seen experimentally. We show this elementary result alongside comparison with experiment to confirm the possibly counter-intuitive conclusion that the effect of centrifugation of a heap on a spinning disk is indeed to reduce compressive stress and increase downstream acceleration as indicated by Eqs. (1) and (2), respectively. This derivation and its confirmation imply that by spinning a granular heap, we effectively counter gravitational acceleration, as defined by Eq. (1). Therefore the technique of spinning a granular heap permits us to probe how grains will behave as compressive stresses are reduced—as occurs for example on the surface of Mars or other small planets.

2 Experiments

2.1 Phase portrait of grains on a spinning disk

Given this simple derivation, one might anticipate that surface patterns would be simple and easily explained as well. Contrary to expectation, a number of unanticipated qualitative and quantitative behaviors appear, which we view as significant and hitherto unrevealed clues to the constitutive behavior of granular flows, especially under reduced gravity conditions.

To investigate these behaviors and their root dependencies, we begin by characterizing how the patterns vary with system parameters, chiefly the mass inflow rate and the disk rotation rate. In the main plot of Fig. 3, we show how pattern selection changes with mass inflow and disk speed. To lowest order, granular behavior is governed by mass conservation [42], and so the ab initio anticipation prior to the experiments that we will describe is that mass inflow should dominate the flows exhibited in our system. Against expectation, we find from Fig. 3 that the patterns produced do not appear to change

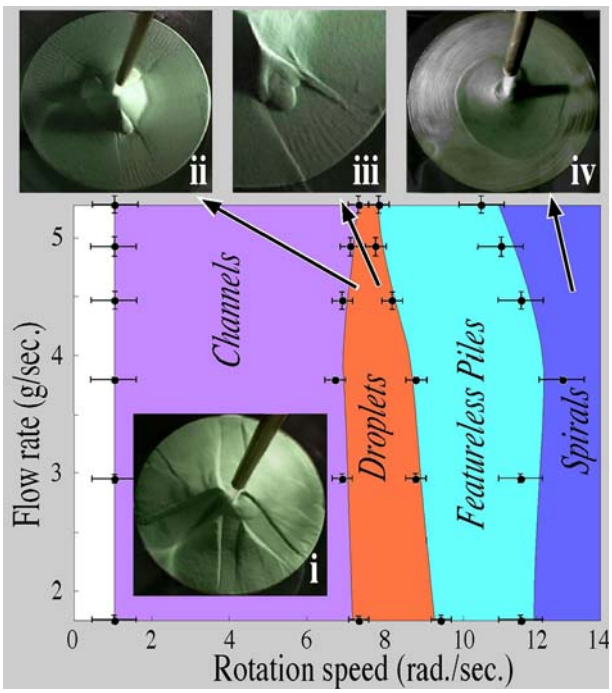

Fig. 3 Parametric dependencies of granular surface patterns on 10 cm diameter spinning disk as a function of inflow rate and rotation rate. There is little dependence on granular inflow rate, but sharp changes from channels to droplets to piles and finally to spirals as rotation rate is increased. *Insets*: *i* Channels: the channels are not precisely uniformly distributed around the disk, but all channels have similar width for a given flow rate. *ii* "Droplet" formation appears spontaneously for weakly cohesive grains, or can be provoked by locally interfering with the flow (see text). *iii* Droplet shapes can become quite elaborate, especially at the higher end of rotation speeds: both droplet patterns shown are steady, but the pattern shown in *iii* is difficult to reproduce and seems to depend significantly on relative humidity. *iv* At very high rotation speeds, the static heap beneath the flowing surface vanishes, and grains flow smoothly and nearly uniformly outward

significantly with inflow rate, but instead exhibit sharp transitions as the disk rotation speed is increased. *This seems*

to represent evidence that reducing compressive loading—which we reiterate occurs in reduced gravity environments—can be expected to have a profound, even dominating, effect on granular flows and pattern formation.

The boundaries shown in the phase portrait are not significantly hysteretic in our experiments, and appear at close to the same locations whether increasing or decreasing rotation speed. Error bars represent standard deviations over multiple (typically 5–10) separate determinations of the transition. In the insets to Fig. 3, we show some of the steady patterns that spontaneously appear, including (i) confined channels, (ii)-(iii) isolated droplets of variable shapes, and (iv) flattened spirals. The precise locations of the transitions between patterns (and even to some degree whether or not a given pattern, e.g., insets (ii) or (iii) discussed next, is present) vary with relative humidity (RH) and wear on the beads. We remark that in the case of the droplet-shaped hillocks of inset (ii), the hillocks themselves are static, and inflowing grains are channeled into steady streams between the hillocks [43]. Occasionally part of a droplet will collapse: collapsed material then flows downstream off of the disk, and the droplet slowly reassembles as material accretes from upstream.

The grains that we use in the results reported here are spherical glass beads, sieved between 75–106 μm. We periodically wash the beads in water, air dry and re-sieve them to remove fine debris, dust and other materials that appear to interfere with reproducibility. Likewise to produce reproducible patterns, we find it necessary to regularly spray all surfaces including the disk and feeder apparatus with antistatic solution. We have also investigated patterns that form using other materials including both larger and smaller glass spheres, hollow glass spheres, sieved crushed glass, sand, lactose powder, and granulated lactose. We have found that channels occur ubiquitously on a spinning disk (though not typically on a stationary one cf. [44,45]), but the more delicate droplets [Fig. 3(ii)–(iii)] are only seen using well-washed, spherical solid glass beads of diameter <100 μm. Other materials typically either flow freely, often in channels, without forming droplets (e.g., larger glass spheres), or clump and form irregular landscapes (e.g., unwashed glass spheres or lactose powder). Other effects of material properties (especially cohesion) on heap fracture on a spinning disk have been studied elsewhere [32].

The disk used in the results shown in this paper is lathed from a single block of acrylic. Experiments were also carried out using polycarbonate and polished steel disks with largely similar results. The disk was driven by a steel shaft that was press-fit into a machined concentric hole coupled to a tachometer-controlled DC motor. Speed fluctuations of the spinning surface were less than 1% as indicated by the tachometer; fluctuations shorter than the motor controller integration time (approx. 1 s) cannot be discounted. Vertical undulations of the disk surface were smaller than could be detected either by eye or by contact with a fixed probe; we estimate these to be well under 1 mm. We have also experimented with disk diameters ranging from 5 to 30 cm in radius. The smallest disks produced only featureless piles, while larger disks (>10 cm radius) generated complex time-varying (e.g., periodically recurring: see Sect. 4) patterns. These merit investigation in their own right, however in this paper we focus on stationary patterns, and so we use a 10 cm radius disk in the work reported here. Other behaviors seen on a non-rotating disk—especially intriguing traveling granular rivers—have been reported elsewhere [43]. We also performed experiments in beakers—i.e., a disk within a bounding cylinder [33,35]. In those experiments, we only observed featureless piles, indicating that the patterns seen are stabilized by accumulation of grains at the downstream edge—presumably this increases collisional dissipation of grains flowing on the surface, though this remains to be confirmed.

The data shown in Fig. 3 are all obtained at $12 \pm 4\%$ RH, $22 \pm 2\,^{\circ}\mathrm{C}$ as measured using a digital hygrometer (Fisher Scientific). Relative humidity (RH) is known to affect interparticle cohesion through the formation of liquid bridges [46,47], and so to investigate the effect of cohesion on pattern formation, we fixed the inflow rate at 3 g/s and repeated the experiments shown in Fig. 3 at $22 \pm 4\%$ RH, $22 \pm 2\,^{\circ}\mathrm{C}$. We found the same transitions, in the same order, but at 20% reduced rotation rate. This result indicates that the transitions are significantly mediated by cohesion. This is in keeping with the general expectation defined by Eq. (3) that centrifuging grains on a spinning disk tends to act counter to compressive stresses, however the specific result that *higher* cohesion corresponds to transitions at *lower* centrifugal accelerations runs *contrary* to expectation, and we do not have a satisfactory explanation for this effect. Our best understanding at this point is that more cohesive grains appear to solidify into channel boundaries or droplets more readily than more freely flowing grains; we return to this point in Sect. 3.2.

2.2 Flow and channels

To explore a sampling of the spectrum of structures that can be produced by granular flows at reduced R_{pt}, we performed variants of the experiments described thus far. As a first case, in Fig. 4a, we recall results of flow on the spinning disk in which grains are fed concentrically and the disk is rotated at 6 rad/s. As shown in the phase plot of Fig. 3, at this rotation rate, the surface exhibits flow in broad, sharp-edged channels. Photographs from Mars occasionally show similar features, for example in the broad channels with nearly vertical banks shown in Fig. 4c. The comparison shown in Fig. 4c is at most qualitative, and is only included to illustrate that broad channels are seen on Mars, yet channeled flows of the kind seen in Fig. 4a are not typical of terrestrial granular systems. We seek therefore to understand why these flows are seen in

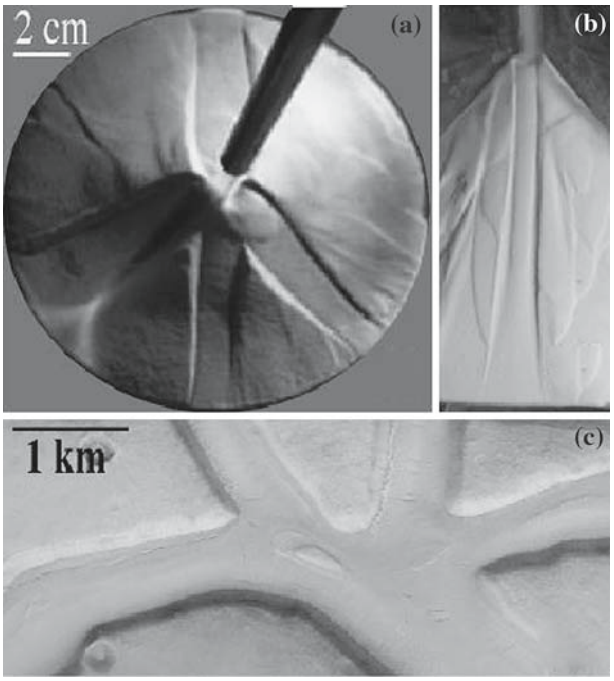

Fig. 4 Channel morphologies in the laboratory and on Mars. **a** Channels on spinning disk, **b** flowing channel formed by small glass beads raining down in a curtain at the upstream edge of the snapshot. **c** Similar aspect ratio channels on Mars, north of Nilosyrtis [51]

the spinning disk, but have not been reported previously in other granular systems.

The theoretical question at issue hinges on the nature of dissipation in granular systems. In a fluid, viscosity is intrinsically velocity-dependent. In a fluid, therefore, as fluid speeds grow under (e.g., gravitational) acceleration, at some point viscous dissipation will increase until it balances the applied acceleration, and a steady, terminal, velocity will be reached. In dry granular systems by contrast, it is not self-evident why either frictional or collisional dissipation leads to velocity dependence—the root cause of this viscous dissipation has been studied both in standard treatments of bulk granular viscosity [48] and in more recent studies of individual granular motions on slopes [49]. The upshot of these analyses is that in order to flow, grains must overcome an initial activation energy to set them in motion, and once in motion they must be resupplied with sufficient collisional energy to remain fluidized [50]. We hypothesize that steady granular streams are supported in the spinning disk because centrifugation accelerates grains downstream and simultaneously reduces their normal compressive load. This hypothesis suggests that similar flows may be generated on a stationary disk by increasing the inflow energy above an activation threshold, below which collisions will cool flowing grains until they stop.

We examine this suggestion in experiments in which fine (30–70 μm), solid spherical glass grains are released from a height of about 10 cm above a heap surface. A characteristic result of these experiments is shown in Fig. 4b. As hypothesized, we find that by releasing grains far above the heap, we can produce a uniform channeled flow that travels as far as we can conveniently accommodate (40 cm in our experiments). To enlarge the heap in the same geometry as is seen in the disk, we construct an acrylic octant with a curved bottom: two sides of the octant are seen near the top of the figure, and the channel flows off of the curved bottom. The presence of significant initial kinetic energy is apparent in Fig. 4b from the fact that the impact of the rapidly falling grains produces an indentation that is visible at the top of the figure. In our experiments, we find that if the incoming stream of grains is released from much closer to the granular surface, grains do not flow steadily, but instead accumulate and release intermittent avalanches that flow a limited distance downslope and then stall.

The channel shown in Fig. 4b develops after a period in which grains initially flow on top of the static heap. This flow thereafter erodes a steep-walled channel into the bed, and once the channel reaches a depth of about 1–2 mm, erosion stops and the flow reaches a steady state. If the inflow is halted, the stream continues briefly on its own inertia and then stops, leaving the channel in roughly the state that appears in the figure. In our laboratory experiments, we see both broad, flat, channels (Fig. 4a, b) and thin, narrow channels with steeply banked borders (reported in [21]). More narrow channels predominate in experiments using angular or cohesive particles [21].

Figure 4b is significant because it illustrates that even in non-rotating frames, grains can flow in uniform and liquid-like streams, however to produce these streams, one must fluidize the grains. This is done in the spinning disk through centrifugal decompression of the heap, and the same is done in the simple heap of Fig. 4b by initiating the stream with sufficiently high kinetic energy grains that they remain fluidized as they flow. In terrestrial experiments, grains of the sizes and densities that we study here will otherwise settle and jam. On the other hand, under reduced gravity conditions, our results (esp. Fig. 3) suggest that enhanced fluidization may occur, and whenever suitable heaps of grains begin to flow, they may continue to flow in a fluid-like state until their source is depleted (cf. [52]).

2.3 Off-center feed

A second feature that we would like to better understand is the droplet shape shown in inset (ii) to Fig. 3. In the experiments shown to this point, the vertical feed tube is centered on the spinning disk, and as we have described, at rotation speeds of 8 ± 1 rad/s and flow rates throughout the range 105–320 g/min, droplet-shaped hillocks form. In this section, we examine the patterns that forms at the same rotation speed and flow rates when the feed tube is place off center with

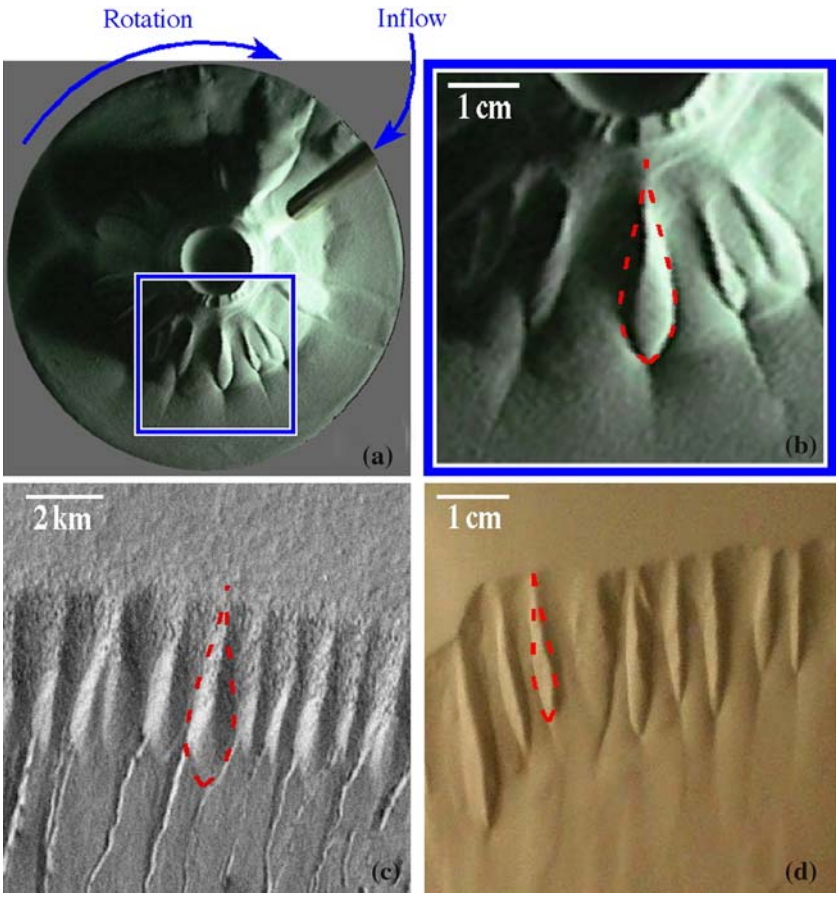

Fig. 5 Rounded hillocks in laboratory experiments **a**, **b**, **d** and on Mars [55] **c**. In **a**–**b**, the hillocks are produced on a rotating acrylic disk onto which glass beads are metered. In **d**, hillocks appear following the collapse of a flat surface of low density hollow beads, discussed elsewhere [21]. The collapse here is provoked by simply tilting the container holding the beads. The red broken lines in **b**–**d** are plots of the same functional form (see text). The crater in the center of **a** is an artefact of the placement of the inflow off of the center of the spinning disk

respect to the disk. The resulting state is shown in Fig. 5. We see that many droplets form around a central caldera. Again, grains flow between static hillocks.

We can estimate changes to the settling-to-flow speed ratio, R_{pt}, on the spinning disk as follows. As shown in Fig. 2b, granular heaps on the spinning disk form an angle of repose of around $\vartheta = 20^\circ$ to the horizontal. On a disk spinning at angular speed ω, the *normal* acceleration imposed by gravity, g, on the heap surface at radius, r, is reduced to $a_n = \mathrm{g} \cdot \cos(\vartheta) - \omega^2 \mathrm{r} \cdot \sin(\vartheta)$, or between about 90% of g near the inside of the disk, and 80% of g, near the outside. At the same time, *tangential* surface accelerations that generate particle flow go as $a_r = \omega^2 \mathrm{r} \cdot \cos(\vartheta) + \mathrm{g} \cdot \sin(\vartheta)$, representing an increase of between 30% near the inside of the disk and 220% near the outside, as compared with accelerations without spinning. Recalling that terminal speeds in a viscous fluid are proportional to the square root of gravitational acceleration [53], these tangential accelerations can increase terminal debris flow speeds by up to 15 or 50%, so on the centrifuging disk, the ratio R_{pt} decreases by 70% near the inside of the disk and by 50% near the outside.

By comparison, the reduction of Martian gravity alone can be expected to diminish R_{pt} on Mars by roughly $1/\sqrt{3}$ or about 60%. When reductions in atmospheric density [54], ρ_a, are taken into account, R_{pt} may be further diminished compared with the terrestrial value. Thus the spinning disk provides a conservative limit to reductions in R_{pt}. Already in this conservative case, features possibly similar to those seen on Mars emerge. In Fig. 5c, we show a photograph [55] of Martian gullies, separated by hillocks that are nearly indistinguishable from the droplets in our spinning disk experiment.

It must be remarked that the spinning disk geometry differs fundamentally from simple slopes in that flows in the streamwise direction necessarily diverge, which is not so for flows down Martian slopes. Therefore to confirm that similar patterns are seen in the absence of the geometric divergence introduced by the rotating disk system, we have also produced similar patterns using hollow beads, which settle slowly due to their low density. One example of a similar pattern is shown in Fig. 5d; channels and rivulets are reported elsewhere [21]. The broken red lines in Fig. 5b–d are all plots of the same function, $y = \pm a x^2\left(1 - x^2\right)$, where x and y are the cross-stream and the down-stream directions, respectively, and a is a fitting constant. Evidently, reducing R_{pt} either by directly changing normal and tangential accelerations (as in the spinning disk experiment) or by changing particle properties (as in prior reduced density experiments [21], also shown in Fig. 5d) has the effect of producing rem-

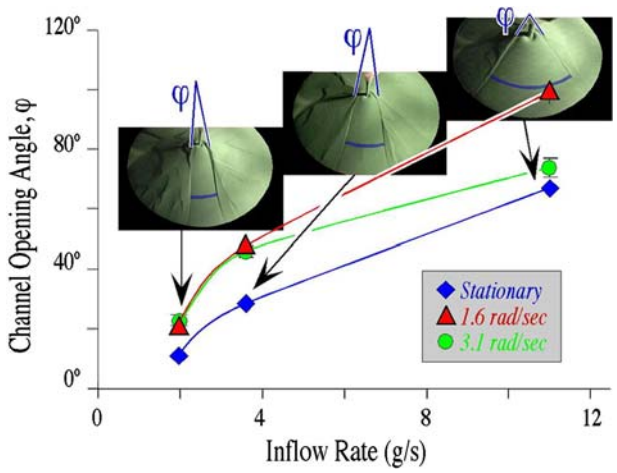

Fig. 6 Growth of channel opening angle with inflow rate at three disk rotation speeds. Insets show typical opening angles at increasing inflow rates. For each flow and rotation speed setting, we evaluate average opening angles using between 6 and 40 channels over three separate experimental realizations. The number of channels measured was chosen to provide comparable standard errors: *error bars* are close to the size of the data markers in this plot. *Lines* are fits to guide the eye

nant structures that are superficially similar to some Martian geomorphic features [56].

2.4 How do channels accommodate flow increases?

We have mentioned that to first order, we would expect that pattern formation would depend strongly on inflow rate, since higher inflows imply greater momentum transfer—thus large avalanches in nature travel further [52], leave more complex deposits [57], and scour deeper channels [58] than smaller avalanches. Since we do not observe significant inflow rate dependence in our experiments, we conclude that the patterns we have reported appear to depend more strongly on the balance between gravitional (compressive) and centrifugal (tensile) stresses within the heap than on momentum balance at the flowing surface.

Nevertheless, simple continuity dictates that flow must depend on mass transport rates, and so we investigate how the granular bed responds to changes in mass flow by performing another set of experiments, summarized in Fig. 6. In these experiments, we vary the inflow rate at three fixed rotation speeds of the disk (indicated in the plot legend) chosen to lie in the channel flow regime, rotation speed $\omega < 7$ rad/s. At each pair of flow and rotation settings, we plot the mean opening angle of the resulting channels.

It is known that the depth of a granular stream does not typically exceed 10–20 grains [41] so the bed must accommodate increases in inflow rates by expanding in a direction other than depth. For example, the grains could accelerate faster in the downstream direction, or the numbers of channels could increase in the azimuthal direction to accommodating a higher inflow. In fact, as shown in the insets of Fig. 6, the bed chooses to accommodate higher inflow rates solely by increasing the opening angle of flowing channels. As the inflow rate is increased (main plot), channels widen from a state in which the channel walls are nearly parallel (left-most inset to Fig. 6) to one in which broadening swathes of grains flow downhill (right-most inset). Again, these are the experimental observations, and we surmise that they must provide clues to granular kinetics underlying these flows, but at the present time, what these clues indicate remains elusive.

3 Analysis

3.1 Dimensional analysis

We begin an analysis of the underlying flow kinetics by performing a Buckingham π dimensional analysis similar to that typically used in fluid flows. The key parameters of the problems are: particle radius (a), particle mass (m), disk radius (R), disk speed (ω), mass inflow rate (q_o), fluid surface tension due to humidity (γ_o), critical angle of repose (ϑ_c), dynamic angle of repose (ϑ_d), and gravitational force on a particle (mg) where g is gravitational acceleration. The density of air is neglected since it is much smaller than that of the grains; air flows may have some effect at higher rotation speeds, but there are no visible effects of air flow below $\omega \sim 7$ rad/s. Above this speed, we see downstream ripples [visible in inset (iii) of Fig. 3] and spirals [inset (iv)] that seem to be associated with air flows, and these may merit further study.

Using the Buckingham π approach, we identify six-dimensionless groups:

(1) a ratio of grain to disk radii, a/R,
(2) a dimensionless flow rate, $q_o/m\omega$,
(3) a ratio of gravitational to centrifugal acceleration, $g/\omega^2 R$.
(4) a granular Bond number, $\gamma_o a/mg$,
(5) the critical angle of repose, ϑ_c,
(6) the dynamic angle of repose, ϑ_d.

We have control over groups (1), (2) and (3), and we can vary (4) by changing the ambient humidity as we have described. This leaves groups (5) and (6) for further analysis. Both of these angles of repose depend in some way on the granular Bond number [group (4)]. As we have shown in Fig. 2b, however, in the spinning disk the *dynamic* angle also depends on the rotation speed [group (3)]. Moreover the droplets of Fig. 4a, b make clear that there is no single *critical* angle of repose in the patterned states either: at the downstream edge of the droplet, this angle is much higher than at its upstream edge. In view of these complications, we seek to investigate

in greater detail how changes in the granular state inter-relate with variations in ϑ_c and ϑ_d.

In particular, a central fundamental question that remains unanswered is whether the patterns seen are signatures of instabilities of granular *flow* or of granular *solidification*. That is, it is possible that a perturbation to a uniformly *flowing* granular layer will cause adjacent regions to, respectively, slow down and speed up, leading to the channels and droplets seen. This would suggest that a traditional instability analysis using a continuum fluid-like model for the granular flow would be appropriate (cf. viscous fingering [59]). It is equally conceivable that a local perturbation in *solidification* between the flowing surface layer and the underlying bed could provoke the local growth of the static bed, leading to the states seen.

To disentangle these two possibilities, we have attempted interventions intended to apply a small perturbation either at the surface (by injecting brief puffs of compressed air onto the flowing surface) or beneath (by sticking small obstacles of clay onto the disk prior to running experiments). Crude though these interventions are, at 8 rad/s, we found no significant changes in the surface pattern in response to puffs of air: this indicates to us that the pattern formation mechanism is robust against applied perturbations to the flow. This indication seems to be supported by the fact that fluctuations in flow rate of up to 10% that we produce by our feeder (Fig. 1) do not interfere with the reproducibility of our experimental results. The response to clay obstacles, on the other hand, was marked: droplets invariably form upstream of any obstacle placed near the outer radius of the heap. This indicates that droplets form in locations where grains stall, suggesting that hysteretic solidification drives the pattern formation process.

This observation leads us to conjecture that the droplet formation is initiated by local condensation (cf. [19,60,61]). This is in accord with our dimensional analysis insofar as the difference between static and dynamic states (corresponding to ϑ_c and ϑ_d, respectively) is what leads to distinct condensed and flowing regions. Furthermore, it is condensation that permits the angle of repose to grow and $g/\omega^2 R$ to become important to the flow. To investigate this conjecture, in the next section we construct a simulation that models both condensed and flowing phases in the spinning disk geometry. For the scope of this paper, we will concentrate only on the formation and mechanism of droplet patterns [Fig. 3(ii)].

3.2 BCRE-inspired cellular automata model

Phenomenological surface granular flows models have been reported and summarized from a variety of perspectives [42,57,62–72]. Currently, there is no continuum model that permits the simulation of both fluid-like and solid-like states on the spinning disk. On the other hand, cellular automata (CA) models of granular flow have a long tradition [73–75]. We implement a CA [76] that is based on the BCRE model

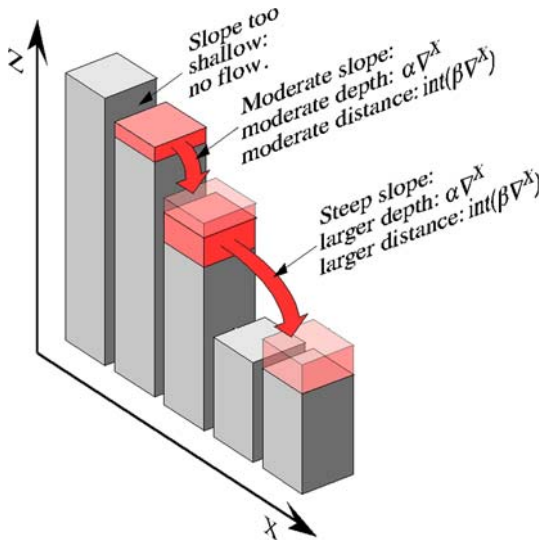

Fig. 7 Schematic of flow in the CA. The amount of material moved downhill and the distance that it is moved both depend on the slope, ∇^X. Here the case for the calculation in the x-direction is shown; a similar process is used for flow in the y-direction

(an abbreviation of the authors' last names Bouchaud, Cates, Ravi Prakash, and Edwards). The BCRE model defines an interface between a flowing layer of grains and a solidified bed beneath, and permits the interface to move up or down so as to account for material transfer between the flowing and static regions.

To construct a CA model in the same spirit, we define a flowing surface layer whose depth depends on the local slope of the free surface. Thus for a steep free surface, a deep layer of grains flows and for a flat free surface, a shallow layer flows. Explicitly, we achieve this by defining a surface height, Z = Z(X,Y,t) at discrete gridpoints (X,Y) and times t. Flow of material is simulated by transferring a quantity $\Delta Z(X,Y)$ in a downhill direction each computational timestep as illustrated in Fig. 7, where downhill is determined by a calculation of the gradient of Z. The gradient is calculated in the X-direction at the grid locations (X_i, Y_j) so that it always points downhill:

$$\begin{aligned} \nabla^X_{i,j} &= \left(Z_{i,j} - Z_{i-1,j}\right) \quad \text{if } Z_{i-1,j} < Z_{i,j}, \text{ or} \\ \nabla^X_{i,j} &= \left(Z_{i,j} - Z_{i+1,j}\right) \quad \text{if } Z_{i+1,j} < Z_{i,j}. \end{aligned} \tag{4a}$$

Similarly in the Y-direction:

$$\begin{aligned} \nabla^Y_{i,j} &= \left(Z_{i,j} - Z_{i,j-1}\right) \quad \text{if } Z_{i,j-1} < Z_{i,j}, \text{ or} \\ \nabla^Y_{i,j} &= \left(Z_{i,j} - Z_{i,j+1}\right) \quad \text{if } Z_{i,j+1} < Z_{i,j}. \end{aligned} \tag{4b}$$

If (X_i, Y_j) is a local maximum, the larger slope is chosen; if it is a local minimum or if both slopes happen to be the same, one is chosen at random.

At each timestep, a quantity, ΔZ, proportional to the slope is removed from a gridpoint (X,Y) and the same ΔZ is added

to the height of another gridpoint downhill at a distance that is, again, proportional to the slope. In this way, the CA explicitly conserves volume: every quantity of material removed from one location is deposited in another, downhill location:

$$\begin{aligned} &Z_{i,j} \rightarrow Z_{i,j} - \alpha\left(\nabla^X_{i,j} + \nabla^Y_{i,j}\right) \quad \text{and} \\ &Z_{i+k^X,j+k^Y} \rightarrow Z_{i+k^X,j+k^Y} + \alpha\left(\nabla^X_{i,j} + \nabla^Y_{i,j}\right). \end{aligned} \tag{5}$$

The distances, k^X and k^Y, at which material is deposited are taken to again be proportional to the local gradient:

$$\begin{aligned} k^X &= k^X_{i,j} = \text{int}\left(\beta \nabla^X_{i,j}\right), \\ k^Y &= k^Y_{i,j} = \text{int}\left(\beta \nabla^Y_{i,j}\right). \end{aligned} \tag{6}$$

In these equations, α and β are the crucial constants of motion: α defines how thick the flowing layer will be, and β defines how far it will travel per unit time (i.e., its velocity). In the simulations that follow, we fix $\alpha = 0.1$ and $\beta = 2$. A schematic of this process is shown in Fig. 7.

We note that k^X and k^Y define distances on a discrete grid and so are necessarily integers. Consequently, if k^X or k^Y is less than the grid spacing, no material will be transported in the corresponding direction. Thus the simulation provides, for free, a critical angle of repose, or gradient, below which flow will stop: this repose angle is defined by $\nabla^X_{i,j} + \nabla^Y_{i,j} = 1/\beta$. To improve the performance of the model, we also include diffusivity, to mimic interparticle collisions, which are ubiquitous in granular flows. Computationally this is simulated merely by adding a small random component to the calculated gradients of Eq'ns [4]. In short, this model is intended to incorporate the analytic framework described by BCRE into the discrete computational approach first introduced by Bak et al. to define self-organized criticality in sandpiles [74].

In the results below, we let grains flow onto a surface consisting of $N \times N$ grid points, with $N = 50$. To initiate droplet formation, we stop the flow at two adjacent grid points at a fixed distance from a center of rotation, which is itself specified as follows. We impose a radial centrifugal force by adding a radially outward term to the gradient at each grid point, where the added term is proportionally to $(\omega^2 \cdot r)$ and has x- and y- components given by $r \cdot \cos\vartheta$ and $r \cdot \sin\vartheta$, respectively. Here, ω^2 is a constant (set at $\omega^2 = 0.2$ in the simulation that follows), and r is the distance of the gridpoint from a fixed, specified rotation center (whose location we will show), and ϑ is the angle of the given gridpoint from

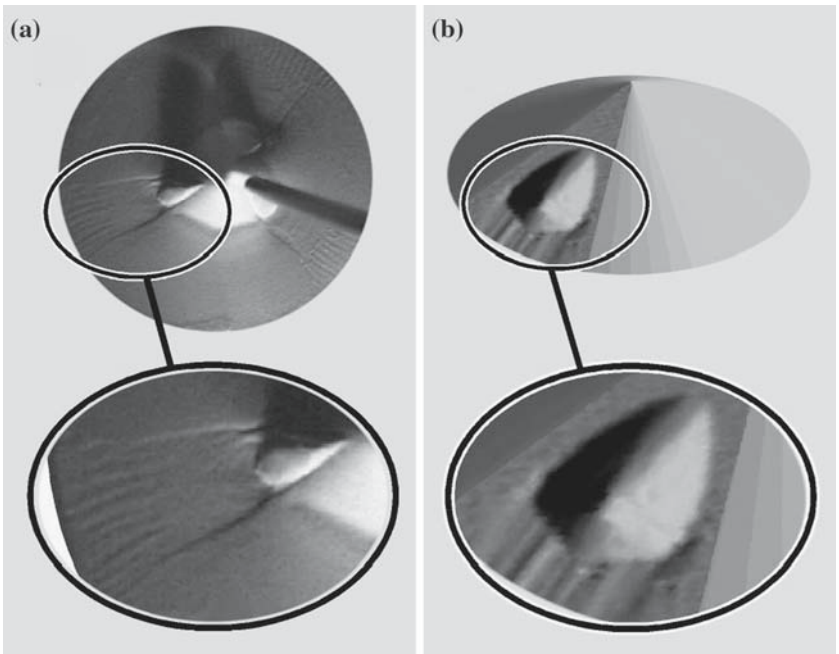

Fig. 8 Experimental and computational localized patterns seen in the spinning disk geometry. **a** An experimental pattern seen at under 8 rad/s. Grains are sieved between 45 and 80 μm, and the mass flowrate is set at 3 g/s, and the disk radius is 9 cm. The droplet-shaped structure is frozen, and grains on either side flow steadily and radially outward. The enlarged inset shows both the droplet shape and the presence of a downstream fan-like wake of the droplet. **b** CA simulation in which a volume-preserving suspension flows downhill under the influence of a body force that is directed radially outward. Only the darker, triangular wedge containing the droplet shape is in the computational domain; the cone outside is included to show where the center of the radial body force originates (see text). The droplet shape and a fan-like wake are produced in this simulation after briefly setting the velocity to be zero artificially at a location under the peak of the droplet. This causes the flow to freeze, and after a short time, the artificial reduction of grain speed is removed. The droplet thereafter forms spontaneously, and as in experiments, the droplet is stationary and flow proceeds around it. In experiments as well we find that droplets can be provoked by placing a small obstacle, e.g., clay, on the spinning disk

a coordinate system with origin at the prescribed rotation center.

We begin simulations with initial heights that are randomized within a small range except at the boundaries, where heights are held fixed. By raising or lowering the fixed height at the boundary, we can externally impose a source or a sink, respectively. This allows us to mimic an inflow upstream and a sink at the edge of the disk, corresponding to our experimental conditions. The same mechanism permits us to computationally impose a localized obstacle that initiates condensation: recall that this was done in our experiments (as described in the previous section) by sticking a small spot of clay onto the disk. Computationally, we initiate condensation by imposing a constant velocity at two adjacent gridpoints, after which grains start to accumulate and pile up—i.e., h(i,j) increases—above the arrested region. After time, h(i,j) evolves into a droplet-like shape, as shown in Fig. 8b; once the droplet begins to form, we remove the constant velocity condition, and the droplet continues to grow until it reaches a final, steady, state as shown in the figure.

In Fig. 8b, we illustrate the origin of the coordinate system (about which centrifugal acceleration is imposed) by artificially sketching a conical pile outside of the wedge-shaped computational region containing the droplet. In Fig. 8a, we show a droplet from one of our experiments. Although the comparison is only qualitative, the apparent ease with which one can reproduce the complex droplet feature suggests that simplified models such as this CA hold significant promise for improved understanding of granular systems possessing both static and flowing regions.

Mechanistically, for the particular example of the droplet shown, the CA model gives support to the hypothesis that *growing condensed regions, rather than a fluid-like flow instability, lead to the droplet patterns* seen in our experiments. This holds two implications. First, our results imply that it is mandatory that models which attempt to capture complex granular features such as we have presented must incorporate transitions between solid-like and fluid-like states, as described by BCRE. Despite recent inroads in this area [19,77,78], it is difficult to adapt continuum models to this task. Second, our results imply that since droplets—and presumably other patterns—are associated with a localized

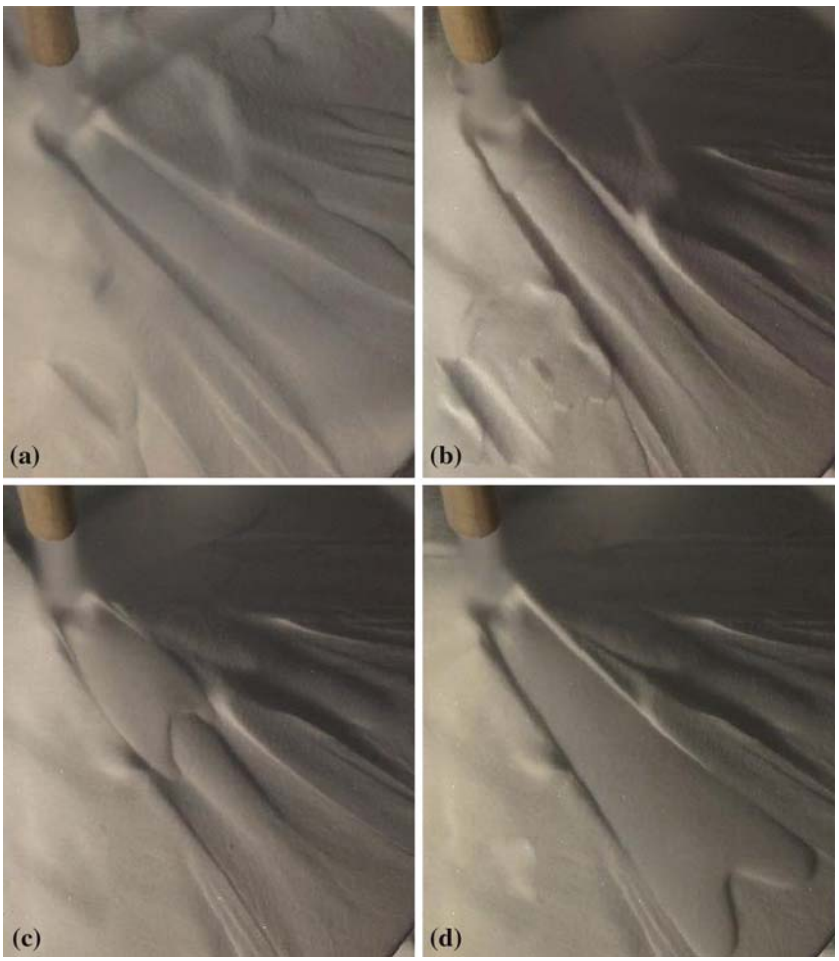

Fig. 9 Time-periodic channel. The disk here is stationary, but is a 25 cm diameter polycarbonate disk, whereas prior figures show flow on a 20 cm diameter acrylic disk

condensation of grains, the patterns expressed may be altered (or removed altogether) by changes to granular properties that affect the readiness with which grains will condense onto a static region. Thus for example we have found in additional experiments (not shown here) that if we increase the particle size—thus decreasing the Bond number and reducing the tendency of grains to form condensates—droplets fail to form at any inflow or rotation rate. In further work, we have found that condensation initiated by electrostatic attraction also provokes granular pattern formation. These results suggest that under reduced gravity conditions, where the Bond number is increased, condensed local structures may be more prevalent than under terrestrial gravity.

Plainly, this type of model has limitations, most significantly it is difficult to directly associate its parameters with measurable particle properties such as size, shape, cohesivity, etc. Nevertheless, the CA that we have described seems to provide an avenue for analysis of intractable problems—such as the spinning disk—in which there are currently few, if any, alternatives that include both the static and flowing regions with sufficient faithfulness to reproduce droplets and other structures. It is, moreover, extremely computationally efficient and permits the analysis of bed behaviors in almost real time. We believe that in the future, simplified models of this type will hold promise for a fuller understanding of the mechanics, dynamics, and evolution of granular materials and flows.

4 Outlook

In conclusion, we have identified a variety of granular flow patterns on a granular heap that change with centrifugal acceleration. Some of the patterns seem to resemble geomorphic structures reported elsewhere from Mars surveys [6] and in a reduced gravity environment [14]. In particular, it is worth noting that recent snapshots from Mars showing before and after photos of channel formation indicate that Martian channels may appear in the absence of surface water (http://www.msss.com/mars_images/moc/2005/09/20/dunegullies/E18-979_S05- 1721sub.gif). The patterned states that we report appear to provide significant clues to intricacies of the granular state. Unexpectedly, we have found that the local solidified patterns displayed do not change appreciably with particle inflow rate, yet depend strongly on the rotation speed of the heap. This indicates that compressive stress—which is strongly dependent on gravity—has a dominant role in solidification behavior, even overcoming first order mass conservation effects. We have also seen that increased flow broadens the widths of flowing channels. It is not at all clear at this point what mechanism underlies this pattern selection effect. Additionally, we have determined that the droplet state appears to be an expression of growth of *local solidification* within the bed, rather than representing a traditional fluid-like flow instability. Finally, we have constructed a flexible CA model that seems to qualitatively capture the static and flowing regions of grains under gravity and centrifugation.

For the future, based on the fact that small, locally condensed, regions in our system grow into unexpected and complex larger patterns, we anticipate that other evolving patterns may also be seen, especially in lower gravity environments where the fluidized state may be prolonged and where local condensation is affected. As one example of such complex temporal evolution, in Fig. 9 we show a final pattern seen in a large (25 cm diameter) disk system. In this figure, we show a periodic state, in which a single channel (a) freezes, and subsequent incoming grains flow toward the outside of the excised channel to produce a double-fingered flow (b–d). After the double-fingers leave the disk, the flow returns to the original state, (a). We believe that the complexity of this periodic pattern is but one of many examples to be revealed in future investigations of this system.

Acknowledgments We thank Jesse Young for technical assistance and initial observations, and the ACS and NSF for financial support.

References

1. Howell, D., Behringer, R.P., Veje, C.: Stress fluctuations in a 2D granular Couette experiment: a continuous transition. Phys. Rev. Lett. **82**, 5241–5244 (1999)
2. Losert, W., Bocquet, L., Lubensky, T.C., Gollub, J.P.: Particle dynamics in sheared granular matter. Phys. Rev. Lett. **85**, 1428–1431 (2000)
3. Menon, N., Durian, D.J.: Particle motions in a gas-fluidized bed of sand. Phys. Rev. Lett. **79**, 3407–3410 (1997)
4. Miller, B., O'Hern, C., Behringer, R.P.: Stress fluctuations for continuously sheared granular materials. Phys. Rev. Lett. **77**, 3110–3113 (1996)
5. Mueth, D.M., et al.: Signatures of granular microstructure in dense shear flows. Nature **406**, 385 (2000)
6. Rabinowica, E.: Friction and wear of materials. Wiley, New York (1965)
7. Treiman, A.H.: Geological settings of Martian gullies: implications for their origins. J. Geophys. Res. **108**, 2002JE001900 (2003)
8. Forterre, Y., Pouliquen, O.: Longitudinal vortices in granular flows. Phys. Rev. Lett. **86**, 5886 (2001)
9. Hanes, D.M., Walton, O.R.: Simulation and physical measurements of glass spheres flowing down a bumpy incline. Powder Technol. **109**, 133 (2000)
10. Louge, M.: Model for dense granular flows down bumpy inclines. Phys. Rev. E **67**, 061303 (2003)
11. Pouliquen, O., Gutfraind, R.: Stress fluctuations and shear zones in quasi-static granular chute flows. Phys. Rev. E **53**, 552 (1996)
12. Pouliquen, O., Renaut, R.W.: Onset of granular flows on an inclined rough surface: dilatancy effects. J. Phys. II (France) **6**, 923 (1996)
13. Savage, S.B., Hutter, K.: The motion of a finite mass of granular material down a rough incline. J. Fluid Mech. **199**, 177 (1989)
14. Silbert, L.E., et al.: Granular flow down an inclined plane: Bagnold scaling and rheology. Phys. Rev. E **64**, 051302 (2001)

15. Bouchaud, J.P., Cates, M.E., Prakash, J.R., Edwards, S.F.: A model for the dynamics of sandpile surfaces. J. Phys. I (France) **4**, 1383–1410 (1994)
16. Bouchaud, J.P., Cates, M.E., Prakash, J.R., Edwards, S.F.: Hysteresis and metastability in a continuum sandpile model. Phys. Rev. Lett. **74**, 1982–1985 (1995)
17. Hsiau, S.S., Hunt, M.L.: Kinetic theory analysis of flow-induced particle diffusion and thermal conduction in granular material flows. J. Heat Transf. **115**, 541 (1993)
18. Komatsu, T.S., Inagaki, S., Nakagawa, N., Nasuno, S.: Creep motion in a granular pile exhibiting steady surface flow. Phys. Rev. Lett. **86**, 1757–1760 (2001)
19. Bocquet, L., Errami, J., Lubensky, T.C.: Hydrodynamic model for a dynamical jammed-to-flowing transition in gravity driven granular media. Phys. Rev. Lett. **89**, 184301 (2002)
20. Liu, A.J., Nagel, S.R.: Jamming is not just cool any more. Nature **396**, 21 (1998)
21. Shinbrot, T., Duong, N.H., Kwan, L., Alvarez, M.M.: Dry granular flows can generate surface features resembling those seen in Martian gullies. Proc. Natl. Acad. Sci. USA **101**, 8542–8546 (2004)
22. Mars: Univ. of Arizona Press, Tucson (1992)
23. Ernst, G.G.J., Sparks, R.S.J., Carey, C.N., Bursik, I.: Sedimentation from turbulent jets and plumes. J. Geophys. Res. **101**, doi: 10.1029/95JB01900 (1996)
24. Fierstein, J.H., Wilson, C.J.N., Hildreth, W.: Complexities of plinian fall depostion at vent: an example from the 1912 Novarupta eruption (Alaska). J. Volcanol. Geotherm. Res. **76**, 215–227 (1997)
25. Pasquero, C., Provenzale, A., Spiegel, E.: A suspension and fall of heavy particles in random two-dimensional flow. Phys. Rev. Lett. **91**, 054502 (2003)
26. Tee, S.Y., et al.: Nonuniversal velocity fluctuations of sedimenting particles. Phys. Rev. Lett. **89**, 054501 (2002)
27. Birnie, D.P.: Rational solvent selection strategies to compat striation formation during spin coating of thin films. J. Mater. Res. **16**, 1145–1154 (2001)
28. Acrivos, A., Shah, M.J., Petersen, E.E.: On the flow of a non-Newtonian liquid on a rotating disk. J. Appl. Phys. **34**, 963 (1960)
29. Emslie, A.G., Bonner, F.T., Peck, L.G.: Flow of a viscous liquid on a rotating disk. J. Appl. Phys. **29**, 858 (1958)
30. Maleki, M., Habibi, M.: Golestanian. Liquid rope coiling on a solid surface. Phys. Rev. Lett. **93**, 214502 (2004)
31. Taylor, D.J., Birnie, D.P.: A case study in striation prevention by targeted formulation adjustment: aluminum titanate sol–gel coatings. Chem. Mater. **14**, 1488–1492 (2002)
32. Genovese, F.C., Watson, P.K., Castellanos, A., Ramos, A.: In: Behringer R.P., Jenkins J. (eds.) Powders and grains. Balkema, Rotterdam (1997)
33. Baxter, G.W., Yeung, C.: The rotating bucket of sand: experiment and theory. Chaos **9**, 631 (1999)
34. Vavrek, M.E., Baxter, G.W.: Surface shape of a spinning bucket of sand. Phys. Rev. E **50**, R3353 (1994)
35. Yeung, C.: Metastability of a granular surface in a spinning bucket. Phys. Rev. E **57**, 4528 (1998)
36. Thomas, P.J.: Pattern formation of granules on the bottom of a differentially rotating tank. J. Fluid Mech. **274**, 23 (1994)
37. Zoueshtiagh, F.: Universal scaling for ripple formation in a granular media. Phys. Rev. E **67**, 031301 (2003)
38. Zoueshtiagh, F., Thomas, P.J.: Wavelength scaling of spiral patterns formed by granular media underneath a rotating fluid. Phys. Rev. E **61**, 5588 (2000)
39. Bird, B.R., Stewart, E., Lightfoot, E.N.: Transport phenomena, 1st edn. Wiley, New York (1960)
40. Melo, F., Joanny, J.F., Fauve, S.: Fingering instability of spinning drops. Phys. Rev. Lett. **63**, 1958–1961 (1989)
41. Brown, R.L., Richards, J.C.: Principles of powder mechanics, 1st edn. Pergammon Press, New York (1970)
42. Herrmann, H.J., Sauermann, G.: The shape of dunes. Phys. A **283**, 24–30 (2000)
43. Altshuler, E., et al.: Sandpile formation by revolving rivers. Phys. Rev. Lett. **91**, 014501 (2003)
44. Börzsönyi, T., Halsey, T.C., Ecke, R.E.: Two scenarios for avalanche dynamics in inclined granular layers. Phys. Rev. Lett. **94**, 2080011–2080014 (2005)
45. Félix, G., Thomas, N.: Relation between dry granular flow regimes and morphology of deposits: formation of levées in pyroclastic deposits. Earth Planet. Sci. Lett. **221**, 197–213 (2004)
46. Duong, N.H., Shen, E., Shinbrot, T., Muzzio, F.J.: Segregation in granular materials and the direct measurement of surface forces using atomic force microscopy. Powder Technol. **145**, 69 (2004)
47. Tardos, G.I., Gupta, R.: Forces generated in solidifying liquid bridges between two small particles. Powder Technol. **87**, 175 (1996)
48. Walton, O.R., Braun, R.L.: Viscosity, granular temperature, and stress calculations for shearing assemblies of inelastic, frictional disks. J. Rheol. **30**, 949–980 (1986)
49. Wolf, D.E., Radjai, F., Dippel, S.: Dissipation in granular materials. Phil. Mag. Ser. B **77**, 1413–1426 (1998)
50. Melosh, H.J.: Acoustic fluidization: a new geological process?. J. Geophys. Res. **84**, 7513–7552 (1979)
51. Malin, M.C., et al.: MOC image E04–02039. Malin space science systems Mars orbiter camera image gallery (2002) http://www.msss.com/moc_gallery/e01_e06/medium_jpg_map/E04/E0402039.jpg
52. Melosh, H.J.: Dynamical weakening of faults by acoustic fluidization. Nature **379**, 601 (1996)
53. Bird, B.R., Stewart, E., Lightfoot, E.N.: In: Transport phenomena, 2nd edn. pp. 61–179. Wiley, New York (2001)
54. Smith, M.D., Pearl, J.C., Conrath, B.J., Christensen, P.R.: One Martian year of atmospheric observations by the thermal emission spectrometer. Geophys. Res. Lett. **28**, 4263–4266 (2001)
55. Malin, M.C., et al.: Polar Pit Wall, MOC2-237. Malin space science systems Mars orbiter camera image gallery (2000) http://www.msss.com/mars_images/moc/june2000/sp_pit/sp_pit_100.jpg
56. Treiman, A.H.: Martian gullies and groundwater: a series of unfortunate exceptions. Lunar Planet. Sci. **XXXVI**, 1713 (2005)
57. Iverson, R.M.: The physics of debris flows. Rev. Geophys. **35**, 245 (1997)
58. Ogden, F.L., Dani, O.R.: Erosional features on Mars surface due to dry mass flows. Preprint (2005)
59. Bensimon, D., Kadanoff, L.P., Liang, S., Shraiman, B.I., Tang, C.: Viscous flows in two dimensions. Rev. Mod. Phys. **58**, 977–999 (1986)
60. Hong, D.C., Quinn, P.V., Luding, S.: Reverse Brazil nut problem: competition between percolation and condensation. Phys. Rev. Lett. **86**, 3423–3436 (2001)
61. Luding, S.: Global equation of state of two-dimensional hard sphere system. Phys. Rev. E **63**, 042201 (2001)
62. Aradian, A., Raphael, E., deGennes, P.G.: Surface flows of granular materials: a short introduction to some recent models. Acad. Sci. Paris **4**, 1 (2001)
63. Bridgwater, J.: Fundamental powder mixing mechanisms. Powder Technol. **15**, 215 (1976)
64. Campbell, C.S.: Rapid granular flows. Ann. Rev. Fluid Mech. **22**, 57–90 (1990)
65. Goddard, J.D., Alam, M.: Shear flow and material instabilities in particulate suspensions and granular media. Part. Sci. Technol. **17**, 69–96 (1999)

66. Jaeger, H.M., Nagel, S.R., Behringer, R.P.: Granular solids, liquids and gases. Rev. Mod. Phys. **68**, 1259–1273 (1993)
67. Jenkins, R.J.: In: Knops, J.T., Lacey, A.A. (eds.) Cambridge University Press, Cambridge (1986)
68. Jenkins, J.T., Savage, S.B.: A theory for the rapid flow of identical, smooth, nearly elastic, spherical particles. J. Fluid Mech. **251**, 187–202 (1983)
69. Johnson, P.C., Nott, P., Jackson, R.: Frictional-collisional equations of motion for particulate flows and their application to chutes. J. Fluid Mech. **210**, 501–535 (1990)
70. Kadanoff, L.P.: Built upon sand: theoretical ideas inspired by granular flows. Rev. Mod. Phys. **71**, 435–444 (1999)
71. Savage, S.B., Lun, C.K.: Particle size segregation in inclined chute flow of dry cohesionless granular solids. J. Fluid Mech. **189**, 311–335 (1988)
72. Savage, S.B., Nedderman, R.M., Tuzun, U., Houlsby, G.T.: The flow of granular materials—III. Chem. Eng. Sci. **38**, 189–195 (1983)
73. Alonso, J.J., Herrmann, H.J.: Shape of the tail of a two-dimensional sandpile. Phys. Rev. Lett. **76**, 4911–4914 (1996)
74. Bak, P., Tang, C., Weisenfeld, K.: Self-organized criticality: an explanation of 1/f noise. Phys. Rev. Lett. **59**, 381–384 (1987)
75. Caglioti, E., Vittorio, L., Herrmann, H.J., Nicodemi, M.: A tetris-like model for the compaction of dry granular media. Phys. Rev. Lett. **79**, 1575–1578 (1997)
76. Shinbrot, T.: Granular coarsening. Granul. Matter **1**, 145 (1998)
77. Gray, J.M.N.T.: Granular flow in partially filled slowly rotating drums. J. Fluid Mech. **441**, 1–29 (2001)
78. Tsimring, L.S., Aranson, I.: Cellular and localized structures in a vibrated granular layer. Phys. Rev. Lett. **79**, 213–216 (1997)